Trapping of palindromic ligands within native transthyretin prevents amyloid formation

Simon E. Kolstoe[a,1], Palma P. Mangione[a,b,1], Vittorio Bellotti[a,b], Graham W. Taylor[a], Glenys A. Tennent[a], Stéphanie Deroo[c,2], Angus J. Morrison[c,3], Alexander J. A. Cobb[c,4], Anthony Coyne[c], Margaret G. McCammon[c], Timothy D. Warner[d], Jane Mitchell[d], Raj Gill[a], Martin D. Smith[e], Steven V. Ley[c], Carol V. Robinson[c,2], Stephen P. Wood[a], and Mark B. Pepys[a,5]

[a]Centre for Amyloidosis and Acute Phase Proteins, Division of Medicine, Royal Free Campus, University College London Medical School, London NW3 2PF, United Kingdom; [b]Dipartimento di Biochimica, Università di Pavia, 27100 Pavia, Italy; [c]Department of Chemistry, University of Cambridge, Cambridge CB2 1EW, United Kingdom; [d]William Harvey Research Institute, Barts and The London Queen Mary's School of Medicine and Dentistry, London EC1M 6BQ, United Kingdom; and [e]Department of Chemistry, University of Oxford, Oxford OX1 3TA, United Kingdom

Edited by David J. Weatherall, University of Oxford, Oxford, United Kingdom, and approved October 7, 2010 (received for review June 14, 2010)

Transthyretin (TTR) amyloidosis is a fatal disease for which new therapeutic approaches are urgently needed. We have designed two palindromic ligands, 2,2′-(4,4′-(heptane-1,7-diylbis(oxy))bis (3,5-dichloro-4,1-phenylene)) bis(azanediyl)dibenzoic acid (mds84) and 2,2′-(4,4′-(undecane-1,11-diylbis(oxy))bis(3,5-dichloro-4,1-phenylene)) bis(azanediyl)dibenzoic acid (4ajm15), that are rapidly bound by native wild-type TTR in whole serum and even more avidly by amyloidogenic TTR variants. One to one stoichiometry, demonstrable in solution and by MS, was confirmed by X-ray crystallographic analysis showing simultaneous occupation of both T4 binding sites in each tetrameric TTR molecule by the pair of ligand head groups. Ligand binding by native TTR was irreversible under physiological conditions, and it stabilized the tetrameric assembly and inhibited amyloidogenic aggregation more potently than other known ligands. These superstabilizers are orally bioavailable and exhibit low inhibitory activity against cyclooxygenase (COX). They offer a promising platform for development of drugs to treat and prevent TTR amyloidosis.

crystallography | mass spectrometry | protein structure | stabilization

Transthyretin (TTR), the normal wild-type (WT) plasma protein that transports thyroxine (T4) and retinol binding protein (RBP), is inherently amyloidogenic, forming microscopic, clinically silent amyloid deposits in the heart and blood vessel walls of most aged individuals (1). Massive cardiac deposition of WT TTR amyloid is a rare cause of intractable heart failure (senile cardiac amyloidosis) (2), and it occurs more commonly with Val122Ile variant TTR that is present in 4% of African Americans (3). More than 80 other single-residue TTR variants cause autosomal dominant, variably penetrant hereditary amyloidosis, affecting about 10,000 people worldwide (4). Disease presents in adult life with various combinations of peripheral and autonomic neuropathy, cardiomyopathy, renal failure, and blindness, and it is fatal within 5–15 y. Liver transplantation, replacing the circulating amyloidogenic variant with WT TTR (5, 6), can arrest progression in younger patients with the common Val30Met variant but is of little benefit in older patients or those with other mutations.

Amyloid fibrillogenesis involves misfolding of native proteins to form partly unfolded intermediates that then aggregate into stable fibrils with the pathognomonic amyloid cross-β core structure (7–9). J. W. Kelly and the company FoldRx, Inc., which he founded, have pioneered use of small-molecule ligands to stabilize the native homotetrameric TTR assembly (10), and their compound, Fx-1006A (tafamidis), is currently in clinical trials (11) (Fig. 1, Compound II). Hitherto, only treatments that substantially reduce abundance of the fibril precursor protein arrest deposition and promote regression of any type of amyloid (6, 12, 13), and we sought to apply this to TTR. The efficacy of specific palindromic, bivalent small-molecule ligands in cross-linking and thereby, depleting circulating serum amyloid P component and C-reactive protein, respectively (14, 15), suggested that TTR might be amenable to the same approach. We selected 2-(3,5-dichlorophenyl amino)benzoic acid (16) (Fig. 1, Compound Ia) as the head group, because it is selectively bound by TTR in whole serum. The TTR bound ligand was reported to have the carboxyl bearing aryl ring buried in the binding pocket and the chlorine bearing ring oriented to the exterior of the protein (17). We, therefore, joined two head groups through their putative external rings so that the palindromic bivalent compound could cross-link two TTR molecules. The initial construct, 2,2′-(4,4′-(undecane-1,11-diylbis(oxy))bis(3,5-dichloro-4,1-phenylene)) bis (azanediyl)dibenzoic acid (4ajm15) (18) (Fig. 1, Table S1), did not cross-link TTR molecules but, unexpectedly, was bound irreversibly under physiological conditions by both native WT and amyloidogenic variant TTR. Furthermore, it stabilized native TTR more potently than monovalent ligands. Based on the crystal structure of the TTR–4ajm15 complex, we designed 2,2′-(4,4′-(heptane-1,7-diylbis(oxy))bis(3,5-dichloro-4,1-phenylene)) bis(azanediyl)dibenzoic acid (mds84) to optimize binding. These compounds reveal an unpredicted and unexpected mode of ligand binding by TTR and create an avenue for treatment of TTR amyloidosis.

Results

Binding of 4ajm15 by TTR. Size exclusion chromatography of isolated native TTR alone and after preincubation in physiological saline with 4ajm15 yielded a single symmetrical peak for each with

Author contributions: S.E.K., P.P.M., V.B., G.W.T., G.A.T., S.D., A.J.M., M.D.S., S.V.L., C.V.R., S.P.W., and M.B.P. designed research; S.E.K., P.P.M., V.B., G.W.T., G.A.T., S.D., A.J.M., A.J.A.C., A.C., M.G.M., T.D.W., J.M., R.G., M.D.S., C.V.R., and S.P.W. performed research; S.E.K., P.P.M., V.B., G.W.T., G.A.T., S.D., A.J.M., T.D.W., J.M., R.G., M.D.S., C.V.R., S.P.W., and M.B.P. analyzed data; and S.E.K., P.P.M., V.B., G.W.T., G.A.T., S.D., M.D.S., C.V.R., S.P.W., and M.B.P. wrote the paper.

Conflict of interest statement: S.E.K., V.B., A.J.M., M.D.S., S.V.L., S.P.W., and M.B.P. are the inventors on patent application WO 2009/040405 A1 on 4ajm15 and mds84, which is owned by Pentraxin Therapeutics Ltd, a University College London spinout company in which S.P.W. and M.B.P. have shares.

This article is a PNAS Direct Submission.

Freely available online through the PNAS open access option.

Data deposition: The crystallography, atomic coordinates, and structure factors have been deposited in the Protein Data Bank, www.pdb.org (PDB ID codes 3IPB, 3M1O, and 3IPE).

[1]S.E.K. and P.P.M. contributed equally to this work.

[2]Present address: Department of Chemistry, University of Oxford, Oxford OX1 3QT, United Kingdom.

[3]Present address: Schering Plough Corporation, Newhouse, Lanarkshire ML1 5SH, United Kingdom.

[4]Present address: School of Pharmacy, University of Reading, Berkshire RG6 6AP, United Kingdom.

[5]To whom correspondence should be addressed. E-mail: m.pepys@medsch.ucl.ac.uk.

This article contains supporting information online at www.pnas.org/lookup/suppl/doi:10.1073/pnas.1008255107/-/DCSupplemental.

Downloaded from https://www.pnas.org by STFC DARESBURY LABORATORY on November 24, 2022 from IP address 193.62.223.243.

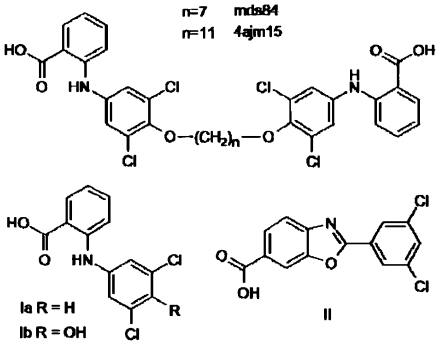

Fig. 1. Structures of TTR binding palindromic ligands mds84 and 4ajm15 together with compound Ia, 2-(3,5-dichlorophenylamino)benzoic acid, originally reported as compound 9 by Purkey et al. (16), compound Ib, 2-(3,5-dichloro-4-hydroxyphenylamino)benzoic acid, and compound II, Fx-1006A.

the same elution volume. The A_{280}/A_{330} absorbance ratio of the peak fraction was ~5:1 compared with 50:1 for TTR alone, and the full UV spectrum was consistent with an ~1:0.9 molar TTR: ligand ratio. 4ajm15 was identified by MS in this fraction, and the complex was stable to freeze-drying and rechromatography.

4ajm15 produced dose-dependent complete displacement of ^{125}I-T4 from both isolated TTR and TTR in whole serum (Table 1 and Fig. 2*A*), showing that 4ajm15 had similar access to both TTR alone and the TTR–RBP complex, which comprises ~20% of circulating TTR. After incubation with whole serum, the presence of 4ajm15 in the TTR immunoprecipitate was confirmed by HPLC-MS (*m/z* 747/9/51, MH^+ and *m/z* 769/71/73, MNa^+).

Intrinsic tryptophan fluorescence of TTR at 300–500 nm on excitation at 280 nm was dose-dependently quenched by 4ajm15 and T4. Emission spectra over 400–600 nm after ligand fluorescence excitation at 340 nm revealed a 480-nm isosbestic point that was associated with progressive tryptophan fluorescence quenching and new 500- to 550-nm emission. Titration with T4 and 4ajm15 reduced intrinsic TTR fluorescence by 40% and 60%, respectively, whereas intrinsic 4ajm15 fluorescence was completely abolished by TTR binding (Fig. 2*B*), consistent with quenching of its emission by simultaneous burial of both head groups of the palindromic ligand within the protein.

MS analysis under mild desolvation conditions revealed that after <1 min preincubation, the minimal time for manual injection of the complex, 4ajm15 was stably bound by WT TTR and the Val30Met and Leu55Pro amyloidogenic variants. Each complex comprised 1:1 molar binding of 4ajm15 by TTR tetramer (Fig. 2*C*). TTR previously complexed at 1:1 and 1:2 molar ratios with *holo* RBP also bound 4ajm15 mole for mole (Fig. 2*D*).

Crystallography of the TTR–4ajm15 Complex. TTR cocrystallized with 4ajm15 showed complex electron density within both hormone binding sites (Fig. 3*A* and Table S2), consistent with the

Table 1. Displacement of T4 from isolated TTR and TTR in whole serum by individual ligands

	IC_{50} (μM) mean ± SD (n = 3)	
	Isolated TTR	TTR in serum
T4	0.10 ± 0.02	0.50 ± 0.1
4ajm15	0.2 ± 0.04	27 ± 4.9
mds84	0.15 ± 0.025	12 ± 1.4
Compound Ia	0.1 ± 0.02	0.6 ± 0.4
Fx-1006A	0.6 ± 0.15	15 ± 4.0

IC_{50}, ligand concentration reducing the binding of ^{125}I–T4 by TTR by 50%.

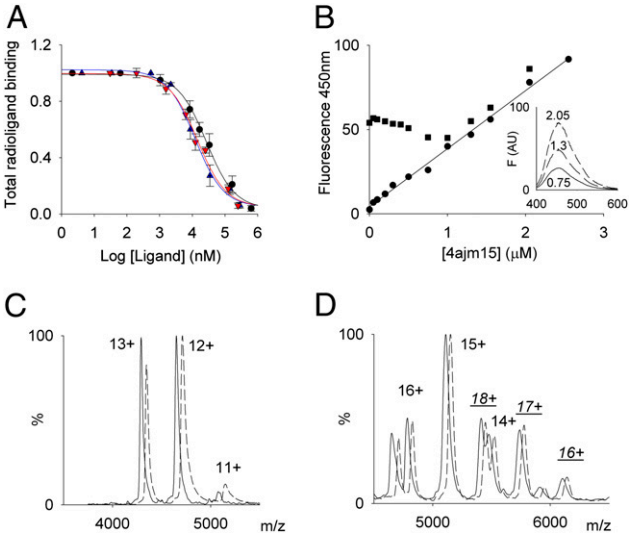

Fig. 2. Ligand binding by TTR. (*A*) Displacement of ^{125}I-T4 from TTR in whole serum by 4ajm15 (●), mds84 (▲), and Fx-1006A (▼). Each point is the mean (SD) of three replicates. (*B*) Emission at 450 nm of 4ajm15 on addition to 1 μM TTR (●) or PBS (■) monitored after excitation at 340 nm. (*Inset*: spectra of 4ajm15 in PBS at three different concentrations.) Nanoflow electrospray mass spectra of WT TTR (*C*) and WT TTR complexed at 1:1 and 1:2 molar ratios with *holo* RBP (*D*) in absence (*apo* WT TTR; solid line) or presence of 1 molar equivalent of 4ajm15 (*holo* WT TTR; dashed line) recorded under nonactivating instrument conditions. The measured mass of *apo* and *holo* TTR is consistent with the binding of 1 mole of 4ajm15 per mole of TTR, even when TTR is complexed with one and two *holo* RBP molecules.

location of chlorinated rings in both the interior and exterior halogen binding sites. There was no electron density for the alkyl linker between them. The inner head group positions were located just 9.5 Å apart, insufficient to accommodate an 11-carbon chain without significant buckling, for which there is inadequate space at the center of the tetramer. The apparent paradox was resolved when a good fit to the electron density was achieved by modeling an 8-Å translational disorder of the bound ligand in addition to the rotational disorder from the crystal symmetry. The extent of this translation corresponded approximately to the excess linker length. Thus, when one head group was ideally fitted to the strong electron density of the inner binding site, the other head group was positioned with chlorine atoms located in the outer halogen binding pockets, and the anthranilate ring was pushed to the weak density at the extremities of the binding site near the outside of the protein (Fig. 3 *A* and *B*). The electron density shows that the chlorinated ring must be rotated by about 90° to relocate between the inner and outer sites. Refinement of this model, with occupancy of 0.25 for each translational and rotational state of the ligand, provided improved refinement statistics and electron density corresponding to the ^{11}C linker passing through the center of the TTR tetramer. In contrast to bound T4 (19), there was no evidence for multiple inner sites, because the local symmetry of the compound matched the crystal symmetry quite closely. However, the anthranilic acid unit occupying the outer part of the pocket showed weakening density distally, and its displacement from the symmetry axis was substantial. This model is in general agreement with that originally proposed by Green et al. (20), who suggested that two bisaryl ligands linked by a 7- to 10-Å alkyl chain would fit comfortably into both T4 binding sites on TTR.

TTR cocrystallized with a single head group (Fig. 1, Ib) closely related to that in 4ajm15 shows chlorines in the inner site (Fig. 3*C* and Table S2), whereas complexes with similar compounds

Downloaded from https://www.pnas.org by STFC DARESBURY LABORATORY on November 24, 2022 from IP address 193.62.223.243.

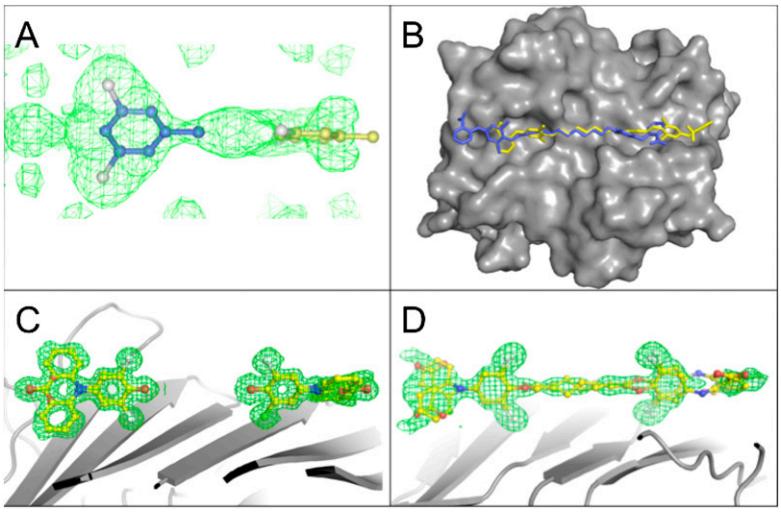

Fig. 3. (*A*) Omit map (contoured at 2σ and 1.9 Å resolution) showing the complex electron density for the contents of one hormone binding site of TTR cocrystallized with 4ajm15 and fitted with two copies [one blue in halogen binding site 1 (HBS1) and one yellow (HBS3)] of the dichorophenyl constituent of the ligand generated by an 8-Å translation and ∼90° rotation. The outer density (yellow model; HBS3) is considerably weaker, and the refined atoms have higher B factors. (*B*) Rendered surface (slate) of the TTR dimer with superposed stick models (blue and yellow) of two complete molecules of 4ajm15 showing the sliding-fit model (Movie S1). (*C*) Electron density (Omit map contoured at 2σ and 1.2 Å resolution) for four molecules of compound Ib (Fig. 1) (one pair of symmetry-related molecules in each binding site) corresponding to the head group of 4ajm15, bound in the forward mode with chlorinated rings toward the center of the TTR tetramer. (*D*) Omit map (contoured at 2σ and 1.4 Å resolution) showing two symmetry-related mds84 molecules bound within the two hormone-binding sites of the TTR tetramer.

produced by soaking ligand into preformed crystals often show the reverse orientation (17). The preferred route of ligand docking into TTR tetramers constrained in the crystal lattice may, thus, involve engagement between the anthranilate carboxyl and Lys15 at the aperture, proceeding to preferential location of the halogens in the outer pockets and internal positioning of the carboxylate.

Development of mds84. To confirm our sliding-fit model for binding of 4ajm15, the bivalent analog with a 7-carbon alkyl linker (Fig. 1), mds84, was prepared. X-ray analysis of the TTR–mds84 complex revealed the chlorinated rings of both head groups in the inner binding site, interconnected by clear electron density corresponding to the 7-carbon linker (Fig. 3*D* and Table S2). The chlorine atoms project to strands G and H of the TTR protomer, and the binding pocket is defined by neighboring peptide main-chain and side-chain atoms derived from symmetry-related subunits (17). The acidic groups approach the terminal side-chain amino groups of Lys15 residues at the binding site entrance. No substantial rearrangement of side-chain positions occurs on binding of these ligands by TTR (Movie S2).

Binding Kinetics of mds84 by TTR. TTR bound mds84 in a 1:1 molar ratio in complexes that were stable on gel filtration and rechromatography after lyophilization. mds84 was slightly more potent than 4ajm15 in displacing bound ^{125}I-T4 from isolated TTR and significantly better in whole serum (Table 1 and Fig. 2*A*). Stopped-flow spectrofluorimetric analysis with isolated TTR showed that mds84 and T4 produced 15% and 50%, respectively, of the ligand-driven quenching of intrinsic protein fluorescence within the lag phase of measurement (<5 ms). The quenching reaction proceeded to completion through a single exponential phase, whose rate constant, with a threefold ligand molar excess, was slower for mds84 (k = 0.094 s^{-1}) than for T4 (k = 0.32 s^{-1}) (Fig. 4). Although k_{on} values could be calculated, estimation of k_{off} for mds84, based on displacement by excess T4, was prevented by the interfering fluorescence of T4 itself. However, MS analysis showed clearly that, after mds84 is bound by TTR, it is not displaced at all, even after incubation for 6 d with 10-fold molar excess of T4 (Fig. 5*A*). In contrast, tafamidis (Fx-1006A) was displaced from the TTR–Fx-1006A complex within 1 min of adding T4 (Fig. 5*A*). The collisional energies required to dissociate TTR-bound Fx-1006A and mds84 were consistent with the T4 displacement results: dissociation starting at ∼1,150 eV for Fx-1006A and ∼1,550 eV for mds84 (Fig. S1).

Stabilization of Native Tetrameric TTR. Spontaneous subunit exchange in TTR under native conditions, well-characterized by MS analysis of TTR mixtures labeled with different isotopes (21), is much swifter and more extensive in the amyloidogenic variants than in WT TTR but was completely prevented by binding of 4ajm15 or mds84 by Leu55Pro TTR, the most unstable variant. With equimolar mds84, exchange was inhibited over many days (Fig. 5*B*); at lower molar ratios, there was some exchange, but TTR with bound mds84 was completely stable (Fig. S2). Complete inhibition of subunit exchange by Fx-1006A required binding of two moles of ligand per mole of TTR and was notably less effective at lower molar ratios (Fig. S3). In competition experiments with mixtures of variant and WT TTR, mds84 was preferentially bound by the variants (Fig. S4). This property

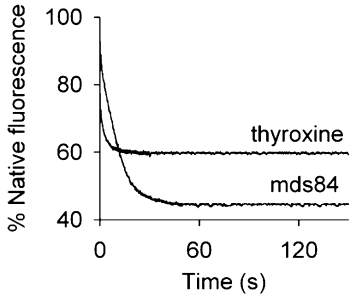

Fig. 4. Kinetics of ligand binding by TTR. Fluorescence emission at 450 nm after excitation at 340 nm of TTR at 2 μM with T4 or mds84 at a threefold molar excess. Results are normalized to 100% fluorescence of the protein alone. The time constant was 11 s for mds84 and 3 s for T4.

Downloaded from https://www.pnas.org by STFC DARESBURY LABORATORY on November 24, 2022 from IP address 193.62.223.243.

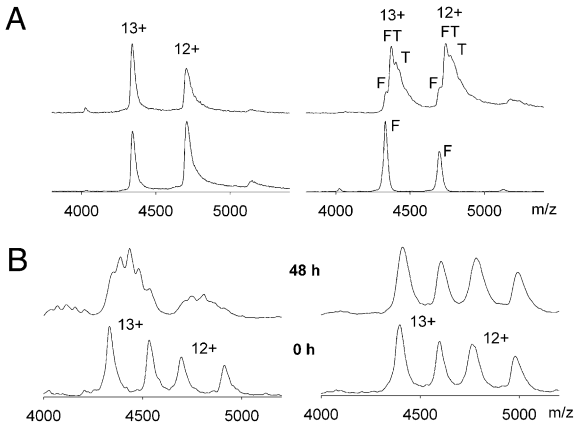

Fig. 5. (*A*) Displacement from TTR of mds84 and Fx-1006A by T4. (*Left*) Mass spectrum of a solution of *holo* WT TTR bound to mds84 before (*Lower*) and 6 d after (*Upper*) the addition of a 10-fold molar excess of T4. In both spectra, the measured mass indicates binding of 1 mole of mds84 per mole of tetramer. (*Right*) Mass spectrum of a solution of *holo* WT TTR with 2 moles of Fx-1006A bound per mole of protein before (*Lower*) and immediately after (*Upper*) addition of a 10-fold molar excess of T4. F designates *holo* TTR bound to two Fx-1006A molecules. Peaks corresponding to the displacement of one and two Fx-1006A molecules by T4 are designated FT and T, respectively. (*B*) Comparison of the subunit exchange in variant Leu55Pro TTR in the presence or absence of mds84. (*Left*) Mass spectra of an equimolar solution containing $^{12}C^{15}N$, and $^{13}C^{15}N$ Leu55Pro variant TTR recorded at time 0 and after 48 h at room temperature; 48 h after mixing, additional peaks in the mass spectrum corresponding to 3:1, 2:2, and 1:3 ($^{12}C^{15}N$:$^{13}C^{15}N$) heterotetramers were observed. (*Right*) Mass spectra of the same equimolar solution of labeled and unlabeled proteins in the presence of a twofold molar excess of mds84. The binding of the ligand completely prevented any subunit exchange occurring in solution.

has not previously been reported for any TTR ligand, whereas several TTR variants, including Leu55Pro (22), have reduced affinity for T4.

The limited solubility of 4ajm15 and mds84 precluded direct measurement of their binding by isothermal titration calorimetry, but differential scanning calorimetry showed marked stabilization of TTR by these ligands. WT TTR alone underwent a single broad asymmetric unfolding transition at pH 7.4 with T_m = 101.3–101.7 °C (23, 24). In the presence of excess 4ajm15 or mds84, the T_m increased by 4.1 °C and 6.2 °C, respectively. The T_m of Leu55Pro TTR was lower than that of the WT, 94.3–94.6 °C (23), but was raised by 5.9 °C in the presence of mds84.

Sedimentation velocity ultracentrifugation analysis of isolated TTR at 3.6 μM and pH 4.4 showed free protomers and large aggregates as well as native tetramer, but in the presence of equimolar 4ajm15, the protein remained tetrameric and sedimented as a single species at 3.7 S, the same effect as a threefold molar excess of T4 under the same conditions. Sedimentation equilibrium analysis of TTR in the presence of 4ajm15 yielded a single species of mass = 55.8 ± 0.1 kDa, consistent with the calculated molecular mass of 55,794 Da of one tetramer bound to one molecule of 4ajm15.

Inhibition of TTR Aggregation. Aggregation at low pH of both WT (pH 4.4) and Leu55Pro variant TTR (pH 5.0), the widely used surrogate for amyloid fibrillogenesis, was profoundly inhibited by 4ajm15 and mds84, which were more potent than Fx-1006A or T4 (Fig. 6).

Pharmacokinetics and COX Inhibition. In mice, i.v. mds84 was eliminated with essentially first-order kinetics over 2 h ($t1/2 \sim 22$ min). It was orally bioavailable and after a single dose was still present in the circulation at 24 h (Table S3). Diclofenac inhibited COX-1 activity in human platelets and COX-2 activity in monocytes with IC_{50} of 55 nM and 27 nM, respectively, but neither mds84 nor 4ajm15 had any COX inhibitory activity at submicromolar concentrations (Fig. S5).

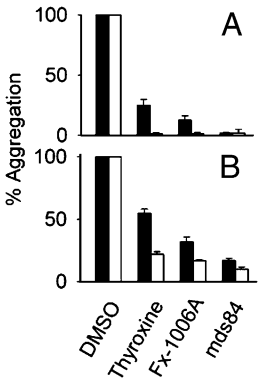

Fig. 6. Inhibition by various ligands of TTR aggregation at low pH. Inhibition of aggregation of WT TTR at pH 4.4 (*A*) and amyloidogenic Leu55Pro variant TTR at pH 5.0 (*B*) by equimolar (solid bars) or threefold molar excess (open bars) of T4, Fx-1006A, and mds84 in solution in DMSO. Each bar shows the mean (SD) of three replicates.

Discussion

Based on our successful previous work with pentraxins (14, 15), we designed a palindromic bivalent ligand, 4ajm15, intended to cross-link TTR molecules and thereby, trigger their depletion from the circulation (18). 4ajm15 did not cross-link TTR but was rapidly bound with high affinity by native TTR and even more avidly by the less stable amyloidogenic variants. Crystallography-based analysis yielded an optimized compound, mds84, which is a very potent TTR superstabilizer.

The remarkable and unprecedented binding of the bivalent ligands, 4ajm15 and mds84, by native TTR and the unusual dynamics are very intriguing. Green et al. (20) considered a threading mechanism and tetramer opening as possible routes for binding, favoring the latter in view of the need for TTR denaturation to permit binding of their bivalent compounds. The normal spontaneous intermolecular exchange of TTR subunits (21, 25) and the high level of hydrogen/deuterium exchange of residues at the subunit interface (26) show the existence of a breathing mode of the protein, which could provide a potential route for ligand entry. However, our palindromic compounds are bound by native TTR much more rapidly than the rate of subunit exchange (21) and are bound even when TTR is in its stable complex with *holo* RBP, which completely prevents exchange of TTR subunits. The scope for disassembly of the tetramer as the permissive event for palindromic ligand binding is, thus, limited for native TTR and favors a threading model where the ligand enters one binding site and crosses the inner channel of TTR. As noted above, some head groups seem to preferentially dock to constrained TTR tetramers in reverse mode, and this would be the only threading option for our palindromic compounds. Progression along such a binding trajectory would require considerable relaxation of the core structure of the TTR tetramer to permit passage of the chlorinated rings. It has previously been reported that the carboxylic group of 3′,5′-difluorobiphenyl-4-carboxylic acid can penetrate the inner channel (27) and perturb the network of hydrogen bonds (28) involving a water molecule, Ser117 and Thr119. Destabilization of the subunit interface in this area and the tendency of the halogen substituents to occupy the inner part of the binding pockets might then provide the driving force for entry of the palindrome. This mechanism should be associated with a conformational change and a transient increase of the free energy of the intermediate binding state, which are then largely compensated by the final si-

Downloaded from https://www.pnas.org by STFC DARESBURY LABORATORY on November 24, 2022 from IP address 193.62.223.243.

multaneous occupation of both binding sites. This hypothesis is consistent with the slower association constant compared with monovalent ligands, the preferential binding by the less stable amyloidogenic variants, and the remarkable strength of binding at the end of the reaction. The apparently critical difference between our palindromic compounds and the bivalent Green compounds that are not bound by native TTR is the presence within 4ajm15 and mds84 of the chlorine atoms. After the palindromic ligand is in place, the large number of ligand-protein contacts stabilizes the complex with binding, which is irreversible under physiological conditions.

The present bivalent ligand compounds have additional desirable features (1). They fully displace T4 from TTR in whole serum at pharmaceutically realistic concentrations but do not compete at all with T4 binding by thryroxine-binding globulin (2). They are preferentially bound by and stabilize amyloidogenic variants, perhaps by virtue of improved access to the ligand site in these molecules, which bind T4 less avidly (22, 29) and are less stable than the WT (3). mds84 does not inhibit COX-1 or COX-2, has good oral bioavailability and a favorable pharmacokinetic profile, and thus, is an attractive platform for drug development.

Materials and Methods

Synthesis of mds84 and 4ajm15. Methyl 2-(3,5-dichloro-4-hydroxyphenylamino) benzoate (1.2–1.4 mmol) was coupled with either dibromoheptane (0.54 mmol) or dibromoundecane (0.43 mmol) in the presence of NaI (10 wt %) and K_2CO_3 (2.7 mmol) in acetone (3 mL) at 60 °C for 12 h. The mixture was purified by silica column chromatography (1:1; petroleum ether/dichloromethane) to afford the dimethyl esters of mds84 and 4ajm15, respectively. The esters were deprotected with 1 M LiOH in 50% methanol:H_2O for 14 h. Full details are in *SI Materials and Methods*.

TTR Preparations. TTR was isolated from normal human serum (30) or purchased (Scipac Ltd). Recombinant human WT and variant (Leu55Pro and Val30Met) TTR, with and without isotopic labeling, were expressed and purified (21, 31). TTR concentrations are expressed as tetramer unless stated otherwise.

T4 Displacement Assays. IC_{50} values for displacement of T4 from isolated TTR and TTR in whole human serum were determined essentially as previously described (32); full details are in *SI Materials and Methods*.

Fluorimetry. Ligands in 100% DMSO were added to 1 μM TTR in PBS, pH 7.4, and monitored in a Perkin-Elmer LS-50B spectrofluorimeter with a 1-cm path-length quartz cell at 20 °C. Binding was detected by quenching of intrinsic protein fluorescence after excitation at 280 nm and quenching of mds84 and 4ajm15 fluorescence emission at 340–600 nm after excitation at 340 nm. Binding kinetics were evaluated by stopped flow (SFM-300; Bio-Logic) with fluorescence detection (Claix) with 2.0-mm cell-path length. Total fluorescence emission over 320 nm, using a cut-off filter, was monitored after 280-nm excitation of 2 μM TTR at 20 °C with threefold molar ligand excess in PBS, pH 7.4, and 5.4% vol/vol DMSO. Kinetic data were acquired as the mean of five experimental mixings. Intrinsic fluorescence quenching data were fitted with a monoexponential function, $y(t) = q + A\exp(-kt)$, where $y(t)$ is the observed fluorescence, q is the fluorescence at equilibrium, A is the amplitude of the observed fluorescence change, and k is the rate constant.

Inhibition of TTR Aggregation. Triplicate aliquots of WT TTR (495 μL; 7.2 μM tetramer) in PBS, pH 7.4, and 0.1% wt/vol NaN_3 were preincubated (37 °C for 30 min) with equimolar or threefold molar ligand excess dissolved in 100% DMSO or DMSO alone; pH was adjusted to 4.4 with 0.2 M NaAc, pH 4.0, and then incubated unstirred (72 h at 37 °C). Leu55Pro variant TTR was studied identically except at final pH 5.0. Absorbance spectra were recorded before and after incubation (DU650 UV-Vis scanning spectrophotometer; Beckman-Coulter). Aggregation was expressed as percent of 400-nm turbidity compared with TTR alone.

Inhibition of COX Activity. Effects on COX-1 and COX-2 activity were determined in comparison with diclofenac (33).

Analytical Ultracentrifugation. TTR (3.6 μM, pH 4.4) was incubated (37 °C for 72 h) with equimolar 4ajm15 or threefold molar T4 excess (34) and then analyzed at 280 nm and 20 °C in the An-50 Ti rotor (XL-I ultracentrifuge; Beckman-Coulter). Sedimentation velocity data were acquired (8 h at 42,000 rpm) in two-sector cells with 12-mm solution column heights and modeled as a continuous distribution of sedimentation coefficients, $c(s)$, using SEDFIT (35). Sedimentation equilibrium results at 17,000 rpm with 100 μL samples in six-sector cells with 2-mm column heights were analyzed using the Beckman software add-on to Origin version 4.1 (MicroCal; GE Healthcare). Partial specific volume of 0.7353 mL/g was calculated from the amino acid sequence (36); buffer density and viscosity were calculated with SEDNTERP (37).

Differential Scanning Calorimetry. The midpoint temperatures of the thermal unfolding transition (Tm) of natural WT and recombinant Leu55Pro TTR were determined in the presence and absence of ligands (MicroCal VP-DSC; GE Healthcare). Thermal denaturation of TTR was irreversible (24, 38), and absolute thermodynamic parameters were not determined.

MS of TTR Ligand Complexes. Nanoflow electrospray mass spectra were recorded (LCT mass spectrometer with Z-spray source; Waters) with capillary voltage of 1.7 kV, sample cone at 80 V, extraction cone at 5 V, ion transfer stage pressure at 5.50 millibar, and time of flight analyzer pressure at 1.75×10^{-6} millibar. Immediately before analysis, fully reduced recombinant TTR preparations were buffer-exchanged into 20 mM NH_4Ac, pH 7.0 (Micro-Bio spin 6 column; Bio-Rad). Equimolar mixtures of $^{12}C^{15}N$-, and $^{13}C^{15}N$-labeled TTR (4.4 μM) in the presence of different molar ratios of ligands in 2.5% vol/vol DMSO or DMSO alone were used to monitor subunit exchange and ligand dissociation. For ligand dissociation experiments, the sample cone voltage was increased stepwise to 200 V. All spectra were calibrated externally using CsI and processed with MassLynx 4.0 (Waters). Human RBP and z-retinol were from Sigma.

Crystallization and X-Ray Analysis. Crystals of TTR–ligand complexes were grown by cocrystallization using hanging drop-vapor diffusion. Drops (6 μL) were composed of 1.5 μL 10 mg/mL TTR, 1.5 μL ligand (10- and 20-fold molar excess), and 3 μL well solution: 25–32% vol/vol PEG550-monomethyl ether, 70 mM NaAc, pH 4–5, 100 mM NaCl. Freeze-dried TTR was dissolved in 10 mM NaAc, pH 5.0, and used immediately. Ligands were dissolved in DMSO and then diluted with 10 mM NaAc, pH 5.0, to the point of precipitation. Final DMSO concentrations in the drop were <12.5% vol/vol. Suitable crystals grew after 2–9 wk and were flash-frozen at 100 K on a nitrogen stream without additional cryoprotectant; X-ray diffraction data were collected at 100 K (station ID14-2; European Synchrotron Radiation Facility and I04 beamline; Diamond) and processed using MOSFLM (39) and CCP4 (CCP4 suite 1994; CCP4). The model was refined with REFMAC5 (40) and Phenix.refine (41), and model building was performed in COOT (42).

Pharmacokinetics of mds84. Pharmacokinetics of mds84 in mice were determined by Medicilon; details are in *SI Materials and Methods*.

ACKNOWLEDGMENTS. We thank Prof. Stephen Perkins (University College London) for help with analytical centrifugation. We gratefully acknowledge access to the synchrotron facilities at European Synchrotron Radiation Facility, Grenoble, France, and Diamond, Oxfordshire, United Kingdom. We thank Ms. Beth Jones for preparation of the manuscript. We also thank Ministero dell'Istruzione Università e Ricerca, Italy (P.P.M.), Fondazione Cariplo and Regione Lombardia, Italy (V.B.), and the Royal Society and Walters-Kundert Trust (C.V.R.) for support. M.G.M. held a Beit Memorial Fellowship. This work was funded by Wellcome Trust Seeding Drug Discovery Award 082989/Z/07/A (to M.D.S., S.V.L., S.P.W., and M.B.P.) and Medical Research Council Program Grant G97900510 (to M.B.P.).

1. Cornwell GG, 3rd, Westermark P (1980) Senile amyloidosis: A protean manifestation of the aging process. *J Clin Pathol* 33:1146–1152.
2. Cornwell GG, 3rd, Murdoch WL, Kyle RA, Westermark P, Pitkänen P (1983) Frequency and distribution of senile cardiovascular amyloid. A clinicopathologic correlation. *Am J Med* 75:618–623.
3. Jacobson DR, et al. (1997) Variant-sequence transthyretin (isoleucine 122) in late-onset cardiac amyloidosis in black Americans. *N Engl J Med* 336:466–473.
4. Saraiva MJ (2002) Hereditary transthyretin amyloidosis: Molecular basis and therapeutical strategies. *Expert Rev Mol Med* 4:1–11.
5. Holmgren G, et al. (1991) Biochemical effect of liver transplantation in two Swedish patients with familial amyloidotic polyneuropathy (FAP-met^{30}). *Clin Genet* 40:242–246.
6. Holmgren G, et al. (1993) Clinical improvement and amyloid regression after liver transplantation in hereditary transthyretin amyloidosis. *Lancet* 341:1113–1116.

Downloaded from https://www.pnas.org by STFC DARESBURY LABORATORY on November 24, 2022 from IP address 193.62.223.243.

7. Booth DR, et al. (1997) Instability, unfolding and aggregation of human lysozyme variants underlying amyloid fibrillogenesis. *Nature* 385:787–793.
8. Sunde M, et al. (1997) Common core structure of amyloid fibrils by synchrotron X-ray diffraction. *J Mol Biol* 273:729–739.
9. Pepys MB (2006) Amyloidosis. *Annu Rev Med* 57:223–241.
10. Johnson SM, et al. (2005) Native state kinetic stabilization as a strategy to ameliorate protein misfolding diseases: A focus on the transthyretin amyloidoses. *Acc Chem Res* 38:911–921.
11. Johnson SM, Connelly S, Wilson IA, Kelly JW (2008) Biochemical and structural evaluation of highly selective 2-arylbenzoxazole-based transthyretin amyloidogenesis inhibitors. *J Med Chem* 51:260–270.
12. Lachmann HJ, et al. (2003) Outcome in systemic AL amyloidosis in relation to changes in concentration of circulating free immunoglobulin light chains following chemotherapy. *Br J Haematol* 122:78–84.
13. Lachmann HJ, et al. (2007) Natural history and outcome in systemic AA amyloidosis. *N Engl J Med* 356:2361–2371.
14. Pepys MB, et al. (2002) Targeted pharmacological depletion of serum amyloid P component for treatment of human amyloidosis. *Nature* 417:254–259.
15. Pepys MB, et al. (2006) Targeting C-reactive protein for the treatment of cardiovascular disease. *Nature* 440:1217–1221.
16. Purkey HE, Dorrell MI, Kelly JW (2001) Evaluating the binding selectivity of transthyretin amyloid fibril inhibitors in blood plasma. *Proc Natl Acad Sci USA* 98: 5566–5571.
17. Oza VB, et al. (2002) Synthesis, structure, and activity of diclofenac analogues as transthyretin amyloid fibril formation inhibitors. *J Med Chem* 45:321–332.
18. Pepys MB, et al. (2009) International Patent Appl WO 2009/040405 A1 (April 2, 2009).
19. Wojtczak A, Cody V, Luft JR, Pangborn W (1996) Structures of human transthyretin complexed with thyroxine at 2.0 A resolution and 3′,5′-dinitro-N-acetyl-L-thyronine at 2.2 A resolution. *Acta Crystallogr D Biol Crystallogr* 52:758–765.
20. Green NS, Palaninathan SK, Sacchettini JC, Kelly JW (2003) Synthesis and characterization of potent bivalent amyloidosis inhibitors that bind prior to transthyretin tetramerization. *J Am Chem Soc* 125:13404–13414.
21. Keetch CA, et al. (2005) L55P transthyretin accelerates subunit exchange and leads to rapid formation of hybrid tetramers. *J Biol Chem* 280:41667–41674.
22. Almeida MR, Saraiva MJ (1996) Thyroxine binding to transthyretin (TTR) variants—two variants (TTR Pro 55 and TTR Met 111) with a particularly low binding affinity. *Eur J Endocrinol* 135:226–230.
23. Shnyrov VL, et al. (2000) Comparative calorimetric study of non-amyloidogenic and amyloidogenic variants of the homotetrameric protein transthyretin. *Biophys Chem* 88:61–67.
24. Takeuchi M, et al. (2007) Destabilization of transthyretin by pathogenic mutations in the DE loop. *Proteins* 66:716–725.
25. Quintas A, Saraiva MJM, Brito RMM (1997) The amyloidogenic potential of transthyretin variants correlates with their tendency to aggregate in solution. *FEBS Lett* 418:297–300.
26. Liu K, et al. (2000) Deuterium-proton exchange on the native wild-type transthyretin tetramer identifies the stable core of the individual subunits and indicates mobility at the subunit interface. *J Mol Biol* 303:555–565.
27. Adamski-Werner SL, Palaninathan SK, Sacchettini JC, Kelly JW (2004) Diflunisal analogues stabilize the native state of transthyretin. Potent inhibition of amyloidogenesis. *J Med Chem* 47:355–374.
28. Blaney JM, et al. (1982) Computer graphics in drug design: Molecular modeling of thyroid hormone-prealbumin interactions. *J Med Chem* 25:785–790.
29. Rosen HN, Moses AC, Murrell JR, Liepnieks JJ, Benson MD (1993) Thyroxine interactions with transthyretin: A comparison of 10 different naturally occurring human transthyretin variants. *J Clin Endocrinol Metab* 77:370–374.
30. Malpeli G, Folli C, Berni R (1996) Retinoid binding to retinol-binding protein and the interference with the interaction with transthyretin. *Biochim Biophys Acta* 1294: 48–54.
31. Lashuel HA, Lai Z, Kelly JW (1998) Characterization of the transthyretin acid denaturation pathways by analytical ultracentrifugation: Implications for wild-type, V30M, and L55P amyloid fibril formation. *Biochemistry* 37:17851–17864.
32. Almeida MR, Damas AM, Lans MC, Brouwer A, Saraiva MJ (1997) Thyroxine binding to transthyretin Met 119. Comparative studies of different heterozygotic carriers and structural analysis. *Endocrine* 6:309–315.
33. Harrington LS, et al. (2008) COX-1, and not COX-2 activity, regulates airway function: Relevance to aspirin-sensitive asthma. *FASEB J* 22:4005–4010.
34. Petrassi HM, Klabunde T, Sacchettini J, Kelly JW (2000) Structure-based design of *N*-phenyl phenoxazine transthyretin amyloid fibril inhibitors. *J Am Chem Soc* 122: 2178–2192.
35. Schuck P (2000) Size-distribution analysis of macromolecules by sedimentation velocity ultracentrifugation and lamm equation modeling. *Biophys J* 78:1606–1619.
36. Perkins SJ (1986) Protein volumes and hydration effects. The calculations of partial specific volumes, neutron scattering matchpoints and 280-nm absorption coefficients for proteins and glycoproteins from amino acid sequences. *Eur J Biochem* 157: 169–180.
37. Laue TM, Shah BD, Ridgeway TM, Pelletier SL (1992) *Analytical Ultracentrifugation in Biochemistry and Polymer Science*, eds Harding SE, Rowe AJ, Horton JC (Royal Society of Chemistry, Cambridge, UK), pp 90–125.
38. Chung CM, Connors LH, Benson MD, Walsh MT (2001) Biophysical analysis of normal transthyretin: Implications for fibril formation in senile systemic amyloidosis. *Amyloid* 8:75–83.
39. Leslie AGW (2006) The integration of macromolecular diffraction data. *Acta Crystallogr D Biol Crystallogr* 62:48–57.
40. Murshudov GN, Vagin AA, Dodson EJ (1997) Refinement of macromolecular structures by the maximum-likelihood method. *Acta Crystallogr D Biol Crystallogr* 53: 240–255.
41. Afonine PV, Grosse-Kunstleve RW, Adams PD (2005) The Phenix refinement framework. *CCP4 Newsletter on Protein Crystallography* 42, contribution 8.
42. Emsley P, Cowtan K (2004) Coot: Model-building tools for molecular graphics. *Acta Crystallogr D Biol Crystallogr* 60:2126–2132.

Downloaded from https://www.pnas.org by STFC DARESBURY LABORATORY on November 24, 2022 from IP address 193.62.223.243.